Hydrodynamic interactions in microphase separation of block copolymer films: Stability and spirals

Y. Shiwa
Statistical Mechanics Laboratory, Kyoto Institute of Technology, Matsugasaki, Sakyo-ku, Kyoto 606-8585, Japan
(Received 3 September 1999; revised manuscript received 27 October 1999)

Effects of hydrodynamic interactions in the formation of lamellar patterns in thin block copolymer films are studied. We derive the phase diffusion equation, and the stability analysis reveals the development of the skewed-varicose instability. Moreover, we predict by means of numerical simulations that the hydrodynamic flow induces the spiral and target patterns.

PACS number(s): 61.41.+e, 47.20.−k, 47.54.+r, 64.60.Cn

In the field of block copolymers (BCPs), the existence of lamellar patterns has been abundantly studied and is now fairly well understood [1]. However, the growth kinetics of the formation of such patterns is much less understood either theoretically or experimentally. This situation bears close analogies with the convective (roll or stripe) pattern formation in a Rayleigh-Bénard (RB) system [2]. For example, the physical mechanism underlying an apparent dynamical scaling regime has not been clearly identified in either system.

In fact, the analogy is not just superficial in these two pattern forming systems, but similar kinetic behaviors can be expected in view of the similarity between the equations governing the dynamics of lamellae and the Swift-Hohenberg model of RB convection. As examples: (i) the dynamical growth of the characteristic length scale in both systems is described by the same growth exponents [3]; (ii) the stability of a lamellar structure and a convective roll gives rise to a common phenomenology [4]. In this paper we explore effects of hydrodynamic interactions in microphase separation of BCP, showing another fascinating connection between the two systems. We predict the appearance of skewed-varicose instabilities and spiral-target patterns in thin BCP films by means of both analytical and numerical investigations.

We consider only an *A*-*B* diblock copolymer with equal-length subchains, in which an ordered layered phase with alternating *A* and *B* rich domains (lamellae) is formed. The model to describe its dynamics is the following time-dependent Ginzburg-Landau (TDGL) equations [5]:

$$\frac{\partial \psi}{\partial t} = L\nabla^2 \frac{\delta H\{\psi\}}{\delta \psi} - (\mathbf{v}\cdot\boldsymbol{\nabla})\psi, \tag{1}$$

$$\rho_0\left(\frac{\partial}{\partial t} - \nu\nabla^2\right)\mathbf{v} = -\mathsf{T}\cdot\left[\psi\boldsymbol{\nabla}\frac{\delta H\{\psi\}}{\delta \psi}\right]. \tag{2}$$

Here $\psi(\mathbf{r},t)$ is the scalar order parameter at a space time point $(\mathbf{r},t)$ chosen to be the local monomer concentration difference of *A* and *B* species. The free energy functional $H\{\psi\}$ is given by

$$H\{\psi\} = \int d\mathbf{r}\left(-\frac{\tau}{2}\psi^2 + \frac{u}{4}\psi^4 + \frac{K}{2}(\boldsymbol{\nabla}\psi)^2\right) + \frac{B}{2}\int\int d\mathbf{r}d\mathbf{r}'\,\psi(\mathbf{r},t)G(\mathbf{r},\mathbf{r}')\psi(\mathbf{r}',t), \tag{3}$$

where G is the Green's function for the Laplace equation, $\nabla_{\mathbf{r}}^2 G(\mathbf{r},\mathbf{r}') = -\delta(\mathbf{r}-\mathbf{r}')$. The $H\{\psi\}$ is essentially the effective Hamiltonian first derived by Leibler and subsequently discussed by Ohta and Kawasaki [6]. The positive constants L,τ,u and K are phenomenological parameters, and $B(>0)$ represents a long-range repulsive interaction and is inherent in the microphase separation. The second term on the right-hand side of Eq. (1) represents the fluid motion. The velocity field $\mathbf{v}(\mathbf{r},t)$ is induced by the hydrodynamic interactions established by the spatially nonuniform distribution of chemical potential, and is assumed to satisfy the incompressibility condition $\boldsymbol{\nabla}\cdot\mathbf{v}=0$. Accordingly the operator T appears in Eq. (2) to select a transverse component of the vector field it is applied to; the ρ_0 and ν are the monomer density and the kinematic viscosity. It is more convenient to take the curl of Eq. (2) to consider the vorticity equation ($\boldsymbol{\Omega}\equiv\boldsymbol{\nabla}\times\mathbf{v}$),

$$\rho_0\left(\frac{\partial}{\partial t} - \nu\nabla^2\right)\boldsymbol{\Omega} = \boldsymbol{\nabla}\frac{\delta H\{\psi\}}{\delta \psi}\times\boldsymbol{\nabla}\psi. \tag{4}$$

Under the assumption that the time scale of $\mathbf{v}$ is much shorter than that of ψ (the so-called ''adiabatic limit'' or ''passive vorticity case''), we set $\partial_t = 0$ in (Eq. 4) as a first good approximation. As a second simplification, which is specific to the thin BCP films, we follow Zippelius-Siggia and Manneville [7] to replace the three-dimensional Laplacian on the left-hand side (LHS) of Eq. (4) by its average over the thickness of the horizontal films. Equation (4) now reads

$$\eta_0(c^2 - \nabla_h^2)\Omega = \boldsymbol{\nabla}\,\delta H\{\psi\}/\delta\psi\times\boldsymbol{\nabla}\psi, \tag{5}$$

where η_0 is the viscosity, and a constant multiplicative factor $-c^2$ arises from the mentioned averaging of ∂_z^2, ∇_h^2 being the horizontal Laplacian, $\nabla_h^2 = \partial_x^2 + \partial_y^2$. Since ∇_h^2 is small when compared to ∂_z^2 in the case of thin films because $c^2 \propto \pi^2/\ell^2$ (ℓ is the vertical thickness of the system) with the proportionality constant depending on the vertical boundary

conditions, we neglect the ∇_h^2 term on the LHS of Eq. (5) in the following stability analysis.

Let us introduce the vertical vorticity potential, ζ, defined by $\hat{\mathbf{z}}\cdot\mathbf{\Omega}=-\nabla^2\zeta$ ($\hat{\mathbf{z}}$ being the unit vector along the z axis) so that $\mathbf{v}=(\partial_y\zeta,-\partial_x\zeta)$. Also hereafter we will use the units in which $u=K=L=1$. Explicitly written, our equations then read

$$\begin{aligned}\partial_t\psi&=\nabla^2(-\tau\psi+\psi^3-\nabla^2\psi)-B\psi-(\mathbf{v}\cdot\boldsymbol{\nabla})\psi,\\ \nabla^2\zeta&=g\hat{\mathbf{z}}\cdot[\boldsymbol{\nabla}(\nabla^2+B\nabla^{-2})\psi\times\boldsymbol{\nabla}\psi],\end{aligned}\tag{6}$$

with $g=1/(c^2\eta_0)$, and $\nabla^{-2}\psi(\mathbf{r})$ is a short-hand notation for $-\int d\mathbf{r}'G(\mathbf{r}-\mathbf{r}')\psi(\mathbf{r}')$. In passing we remark that generally for BCP with asymmetric chains the ψ's in the long-range interaction term in the free energy (3) are replaced by $\delta\psi(\mathbf{r})\equiv\psi(\mathbf{r})-\overline{\psi}$, where $\overline{\psi}$ is the spatial average of ψ; $\overline{\psi}=0$ for symmetric chains. Therefore the $\mathbf{k}=\mathbf{0}$ mode (i.e., the Fourier components $\psi_{\mathbf{k}}$ for $\mathbf{k}=\mathbf{0}$) is a constant of motion ($\psi_{\mathbf{k}=\mathbf{0}}=0$) with the form of the first equation of Eq. (6), and the order parameter ψ is a conserved quantity.

We here employ the method of phase dynamics [8] to seek slowly-varying (slow reorientation of the lamellae over large angles) and finite-amplitude (far from threshold) lamellar solutions to the governing equations (6). To that end one introduces slow space and time variables

$$X=\eta x,\quad Y=\eta y,\quad T=\eta^2 t,\tag{7}$$

and a slow phase variable

$$\Theta(X,Y,T)=\eta\theta(x,y,t).\tag{8}$$

The only small (dimensionless) parameter η in the analysis is the ratio of lamellar size to system size, and the local wavevector of lamellae is given by

$$\mathbf{k}(X,Y,T)\equiv\boldsymbol{\nabla}\theta=\boldsymbol{\nabla}_{\mathbf{X}}\Theta,\tag{9}$$

where $\mathbf{X}=(X,Y)$, and k is $O(1)$. We develop the solution as an expansion in η:

$$\begin{aligned}\psi&=\psi_0+\eta\psi_1+\cdots,\\ \mathbf{v}&=\mathbf{v}_0+\eta\mathbf{v}_1\cdots,\\ \zeta&=\zeta_0+\eta\zeta_1+\cdots,\end{aligned}\tag{10}$$

where $\psi_i=\psi_i(\theta=\eta^{-1}\Theta(X,Y,T),X,Y,T)$, etc, are 2π-periodic in θ. One may then match the result to $O(\eta^2)$. Since the calculation may be carried out in exactly the same way as in Refs. [4,9], we skip details here.

At order η^0, we obtain the equation

$$0=\hat{O}\psi_0\equiv(\tau k^2\partial_\theta^2+k^4\partial_\theta^4+B)\psi_0-k^2\partial_\theta^2\psi_0^3\tag{11}$$

giving the unperturbed solution ψ_0. At $O(\eta)$, we obtain the linear equation for ψ_1,

$$\delta\hat{O}\psi_1=-F_1,\tag{12}$$

where $\delta\hat{O}$ is the operator obtained by linearizing the operator $\hat{O}$ about ψ_0,

$$\begin{aligned}\delta\hat{O}=\tau k^2\partial_\theta^2+k^4\partial_\theta^4+B-k^2[&3\psi_0^2\partial_\theta^2+12\psi_0(\partial_\theta\psi_0)\partial_\theta\\&+6\psi_0(\partial_\theta^2\psi_0)+6(\partial_\theta\psi_0)^2].\end{aligned}\tag{13}$$

The right-hand side of Eq. (12) contains all terms involving ψ_0,

$$\begin{aligned}F_1=\Theta_T\partial_\theta\psi_0+\tau D_1\partial_\theta\psi_0+k^2\partial_\theta^2 D_1\partial_\theta\psi_0+D_1\partial_\theta k^2\partial_\theta^2\psi_0\\-12\psi_0\mathbf{k}\cdot(\boldsymbol{\nabla}\psi_0)\partial_\theta\psi_0-3\psi_0^2 D_1\partial_\theta\psi_0+(\mathbf{v}_1\cdot\mathbf{k})\partial_\theta\psi_0.\end{aligned}\tag{14}$$

Here and hereafter $\boldsymbol{\nabla}\equiv\boldsymbol{\nabla}_{\mathbf{X}}$, and $D_1\equiv 2\mathbf{k}\cdot\boldsymbol{\nabla}+(\boldsymbol{\nabla}\cdot\mathbf{k})$, $\Theta_T\equiv\partial_T\Theta$. For slowly varying component of the vertical vorticity potential, the only contibution to the flow $\mathbf{v}$ at $O(\eta)$ is the part with no dependence on the fast scale θ,

$$\mathbf{v}_0=0,\quad \mathbf{v}_1=(\partial_Y\zeta_0,-\partial_X\zeta_0).\tag{15}$$

We find the θ-independent components of the vorticity potential $\zeta_0=\zeta_0(X,Y)$ by averaging the $O(\eta^2)$ of the vorticity equation over θ to give

$$\begin{aligned}\nabla^2\zeta_0=-g\hat{\mathbf{z}}\cdot\{\mathbf{k}\times\boldsymbol{\nabla}\boldsymbol{\nabla}\cdot[\mathbf{k}\langle(\partial_\theta\psi_0)^2\rangle]-B\mathbf{k}\\\times\boldsymbol{\nabla}[k^{-4}\boldsymbol{\nabla}\cdot(\mathbf{k}\langle(\partial_\theta^{-2}\partial_\theta\psi_0)^2\rangle)]\}.\end{aligned}\tag{16}$$

Here the scalar product $\langle a,b\rangle$ is defined by $\langle a,b\rangle=(2\pi)^{-1}\int_0^{2\pi}d\theta ab$, and $\langle a^2\rangle=\langle a,a\rangle$. The operator ∂_θ^{-2} is defined by

$$\partial_\theta^{-2}\phi(\theta)=-\int d\theta' G^*(\theta,\theta')\phi(\theta'),\tag{17}$$

where $\partial_\theta^2 G^*(\theta,\theta')=-\delta(\theta-\theta')$. The phase equation for $k(\Theta)$ arises as solvability condition for Eq. (12), $\langle e_0^\dagger,F_1\rangle=0$, where $e_0^\dagger$ is the zero-eigenvalue eigen function of the adjoint to $\delta\hat{O}$. At this stage we employ an approximation to use a single-mode truncation of ψ_0 as

$$\psi_0=A\cos(\mathbf{k}\cdot\mathbf{x}).\tag{18}$$

The one-mode truncation has been shown to be a good approximation in the stability analysis of a large class of model equations in thermal convection [9]. With the one-mode truncation, $e_0^\dagger$ is simply given by $e_0^\dagger=\sin(\mathbf{k}\cdot\mathbf{x})$. Then we obtain the phase equation for small long-wavelength perturbations from uniform lamellae with wavevector $\mathbf{k}=(k,0)$,

$$\omega^{-1}(k)(\Theta_T+\delta\Theta_T)=D_\parallel(k)\Theta_{XX}+D_\perp(k)\Theta_{YY}.\tag{19}$$

Here

$$\begin{aligned}D_\perp(k)&=(1/2)A^2k_0^2(K^2-K^{-2}),\\ D_\parallel(k)&=\frac{2}{3}k_0^4\frac{K^4+3}{K^2}\left[\epsilon-\frac{3K^8-2K^6-6K^2+5}{K^2(K^4+3)}\right],\end{aligned}\tag{20}$$

with

$$\omega^{-1}(k)=A^2/2,\quad A^2=(4k_0^2/3)(\epsilon+2-K^2-K^{-2}),\tag{21}$$

and $K \equiv k/k_0$; k_0 and ϵ are, respectively, a critical wavenumber and a reduced distance to criticality given by

$$k_0 = B^{1/4}, \quad \epsilon = (\tau - 2k_0^2)/k_0^2. \tag{22}$$

The characteristic feature of the phase equation (19) is the term $\delta\Theta_T \equiv k\partial_Y \zeta_0$, which is absent without hydrodynamic interactions, and

$$\delta\Theta_T = -\omega(k)\alpha(k)\Theta_{YY} - \omega(k)\beta(k)\nabla^{-2}\Theta_{XXYY}, \tag{23}$$

where

$$\alpha(k) = (1/4)A^4 g_m (K^2 - K^{-2}),$$
$$\beta(k) = -(2/3)A^2 k_0^2 g_m (K^2 - K^{-2})^2, \tag{24}$$

with $g_m \equiv g k_0^2$. In order to derive Eq. (23), we have used the fact that the Green's function for the operator $\mathcal{L}: \mathcal{L}y(\theta) = d^2 y(\theta)/d\theta^2$ and the periodic boundary conditions $y(0) = y(2\pi), y'(0) = y'(2\pi)$ is given by [10]

$$G^*(\theta, \theta') = \frac{\pi}{6} - \frac{1}{2}|\theta - \theta'| + \frac{1}{4\pi}(\theta - \theta')^2. \tag{25}$$

Therefore the hydrodynamic coupling leads to the modified phase-diffusion equation of the form

$$\omega^{-1}(k)\Theta_T = D_\parallel(k)\Theta_{XX} + \tilde{D}_\perp(k)\Theta_{YY} + \beta(k)\nabla^{-2}\Theta_{XXYY}, \tag{26}$$

where $\tilde{D}_\perp(k) = D_\perp(k) + \alpha(k)$.

The growth rate (Λ) of a small perturbation of wave vector $\mathbf{Q} = Q(\cos\phi, \sin\phi)$ about a straight lamella of $\mathbf{k} = (k, 0)$ (hence ϕ is the perturbation angle to the layer normal) is determined by a linear stability analysis of Eq. (26):

$$\Lambda/[Q^2\omega(k)] = -[D_\parallel(k)\cos^2\phi + \tilde{D}_\perp(k)\sin^2\phi + \beta(k)\cos^2\phi \sin^2\phi]. \tag{27}$$

For fluctuations with $\phi = 0$, the longitudinal Eckhaus (EC) instability [2] occurs if $D_\parallel(k) < 0$, and this stability boundary is unchanged by the hydrodynamic coupling ($g_m \neq 0$). For $\phi = \pi/2$, the transverse zigzag (ZZ) instability develops if $\tilde{D}_\perp(k) < 0$. The vorticity generated by the hydrodynamic interaction acts as a stabilizing influence on the ZZ instability inside the neutral stability region where $A^2(k) > 0$. However, the influence is not strong enough to change the stability boundary as compared to the case of $g_m = 0$. For $\mathbf{Q}$ at some orientation $0 < \phi < \pi/2$, the vorticity is destabilizing because $\beta(k) < 0$, and a new instability is induced. Namely, the local changes in lamellar spacing ($Q_x \neq 0$) coupled with lamellar bending ($Q_y \neq 0$) enhance the bulges. This flow-driven instability may be identified as the skewed-varicose (SV) type, a familiar instability in thermal convections at low Prandtl numbers.

In this connection the following remark may be in order. The BCP (or RB) system consisting of fully formed lamellae (or rolls) has the same symmetry as a smectic liquid crystal, and we thus expect similar behaviors in the latter system. In fact, two-component smectics *A* undergoing a demixing transition to the two coexisting smectic phases bear some resemblance, where the elastic degrees of freedom (the layer displacement fluctuations) are coupled to the concentration. In terms of linearized smectic hydrodynamics, Sigaud *et al.* [11] interpreted the fastest growing mode of the two-component smectics quenched below the spinodal as arising from the instability of a diffusive baroclinic mode. The layer displacement in this mode exhibits a novel pattern similar to Fig. 3(a) below, and the angle between the most unstable wave vector and the layer normal is predicted to be near $\pi/4$ [see the comment on Eq. (28) below]. Therefore this appears to be the exact analogue of the SV instability that we have described.

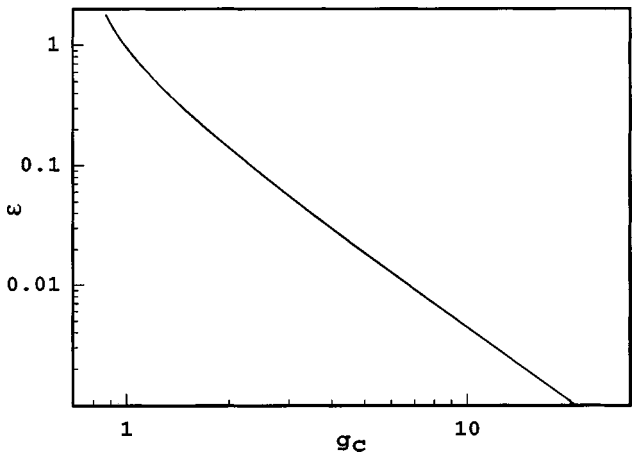

FIG. 1. The g_c as a function of ϵ. For a given ϵ, the hydrodynamic coupling with strength $g_m > g_c$ generates the skewed-varicose instability.

Studying in detail the growth rate (27), we find that the SV instability grows continuously out of the EC instability both for increasing ϵ and for increasing g_m. For a given ϵ, the hydrodynamic interactions with $g_m > g_c(\epsilon)$ generate the SV instability, whereas for $g_m < g_c$, the EC instability preempts the SV instability. Figure 1 shows the variation of g_c

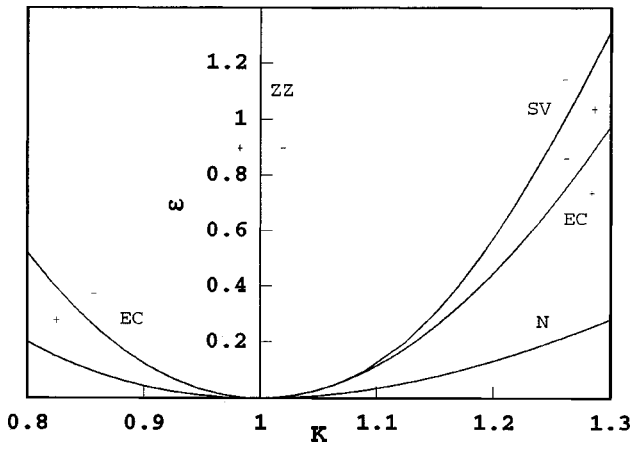

FIG. 2. Stability boundary for $g_m = 10$ as a function of ϵ and the reduced wave number *K* (ZZ: zigzag; SV: skewed-varicose; EC: Eckhaus; N: neutral instabilities). The plus and minus signs on either side of a curve show where the growth rate (Λ) is positive or negative; hence only the region labeled with two minus signs is stable. Although it is illegible in the figure on this scale, the EC instability preempts the SV instability for $\epsilon < 0.0044$ and $1 < K < 1.02$.

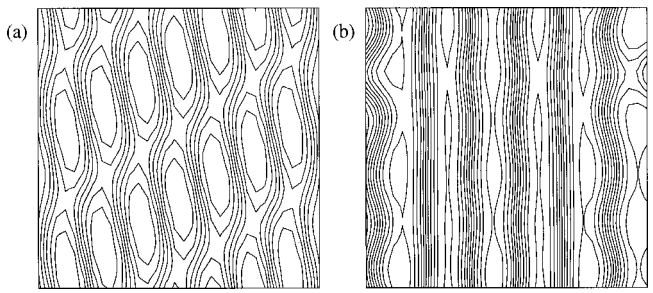

FIG. 3. (a) Initial phases (at 500 time step) of the skewed-varicose instability in the simulation on a grid of 32×32 mesh points. The horizontal axis is the x axis. Contour lines are equally spaced and represent the value of $\psi(|\psi|<1.1)$; (b) Here the ZZ as well as SV modulations are visible. The initial state for the evolution is chosen to be $\psi(i,j)=\cos(0.95k_0 i\Delta x)+\cos(0.1j\Delta y)$, and all other parameters used are the same as in (a) while $|\psi|<0.67$.

with ϵ. A representative stability diagram (we used the value $g_m=10$) is summarized in Fig. 2, showing the various stability boundaries as a function of ϵ and the scaled wave vector K. The stable region is bounded mostly by the ZZ and SV instabilities for this value of g_m.

We have undertaken numerical simulations of the coupled equations (6) to provide the checks on the analytical predictions of our stability analysis. The numerical results to be presented were obtained by discretizing both space and time derivatives in equations (6). Euler's method was used to discretize the time derivative and the discrete gradient was center difference evaluated. The discrete Laplacian used the so-called CDS Laplacian [12] including contributions from nearest and next-nearest neighbors with relative weight 1 and 1/2. A standard fast-Fourier transform technique solved the vorticity equation. We take as initial condition

$$\psi(i,j)=\cos(1.155k_0 i\Delta x)+0.5\cos[0.5(i\Delta x+0.8j\Delta y)], \tag{28}$$

where the integers (i,j) represent the coordinates (x,y); $x=i\Delta x, y=j\Delta y$. We use $\tau=1$, $B=0.189$, $g=23$ (hence $g_m=10$, $k_0=0.66$ and $\epsilon=0.3$) for our simulations performed with periodic boundary conditions. The grid spacing of $\Delta x=\Delta y=1.0$ and the time step size $\Delta t=0.01$ are chosen to avoid numerical instabilities. [The value 0.8 in the above equation corresponds to the value of $\tan(Q_y/Q_x)$ which maximizes the growth rate for the SV instability for the parameters chosen for our simulation.] Since we are outside of the stability region (see Fig. 2), we expect to observe the SV instability. In Fig. 3(a) we exhibit the initial phases of the SV instability. It is evident that the mean drift field caused by the vorticity coupling enhances the necking of phase contours. We also observed the ZZ instability with the other appropriate choice of initial conditions [Fig. 3(b)], and all our simulations were fully quantitatively consistent with analytical theory.

At this juncture we recall recent surprising observations of spiral or target patterns in RB convection [13]. These intriguing patterns were observed in a parameter region where the familiar state of parallel-roll pattern is known to be stable. Although a full theoretical understanding of the mechanism responsible for these patterns is lacking, it is currently postulated that the patterns are due to the large-scale flow (so-called mean flow) generated by the deformation of convective rolls [14]. Realizing that the mean flow arises when vertical vorticity is driven by roll curvature and amplitude modulations [15], and considering the similarities between RB convection and BCP, we explore parallels between these two systems. A natural question then is whether spirals or targets are observed in BCP. Below we suggest by means of numerical simulations that these patterns occur for strong hydrodynamic coupling and large systems.

We have carried out simulations based on Eqs. (1, 5). In order to allow easier exploration of the long-time regime of pattern formation, we employed the cell-dynamical-system (CDS) method [16,5] on square lattices with periodic boundary conditions. For Eq. (1), i.e., the first of equations (6), we solved the following CDS model:

$$\psi(\mathbf{n},t+1)=\psi(\mathbf{n},t)-\langle\langle[\mathcal{J}(\mathbf{n},t)\rangle\rangle+\mathcal{J}(\mathbf{n},t)-\tilde{B}\psi(\mathbf{n},t) -\mathbf{v}(\mathbf{n},t)\cdot[\boldsymbol{\nabla}]_d\psi(\mathbf{n},t), \tag{29}$$

where $\mathcal{J}=A\tanh\psi+D(\langle\langle\psi\rangle\rangle-\psi)-\psi$, corresponding to the effective chemical potential $-\delta H/\delta\psi$. For the strength of the long-range interaction we have used the different notation $(\tilde{B})$ in Eq. (29) from the TDGL model, since in comparing Eqs. (6) and (29) a suitable rescaling of variables is necessary to allow for the different units used in CDS and TDGL dynamics. In Eq. (5) all the operators are replaced by their discrete counterparts. Explicitly, this gives us

$$(c^2-[\nabla^2]_d)[\nabla^2]_d\zeta=g\hat{\mathbf{z}}\cdot\{[\boldsymbol{\nabla}]_d(D(\langle\langle\psi\rangle\rangle-\psi)+\tilde{B}[\nabla^{-2}]_d\psi) \times[\boldsymbol{\nabla}]_d\psi\}. \tag{30}$$

In the above the double angular brackets denote an isotropized average of a neighborhood of cells, and $[*]_d$ denotes the discrete version of the enclosed operator; the discrete

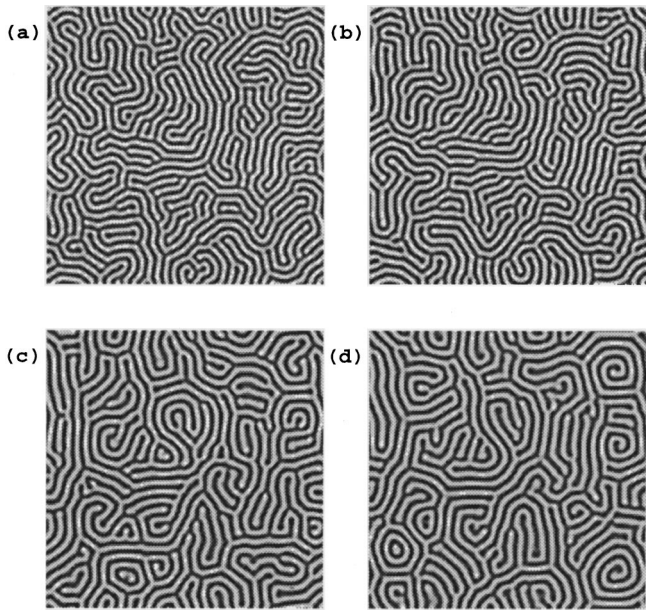

FIG. 4. Patterns at 10^4 time step after random initial conditions in a system of size 256×256 showing the variation of patterns as the hydrodynamic coupling strength is changed; $g=0.25$ (a), 2.5 (b), 25 (c), and 50 (d). The bright regions denote positive values of ψ while the dark ones negative ψ.

gradient was center difference evaluated and for the Laplacian we used the identification [12] $[\nabla^2]_d * = 3(\langle\langle * \rangle\rangle - *)$. The operator $[\nabla^{-2}]_d$ is the inverse of the discrete Laplacian $[\nabla^2]_d$, and is computed using fast Fourier transform techniques. The parameters used were $A=1.26$, $\tilde{B}=0.02$, $D=0.45$ and $c^2=2$ at variable values of g. Initial conditions were a random distribution between ± 0.1. We have studied several systems of size 64^2 to 256^2 to investigate the size dependence of possible patterns. The conclusions that we can draw from the simulations are (i) The spirals are found to exist only for large hydrodynamic coupling. (ii) Spirals and target can coexist. (iii) The spiral disappears in a small system of size 64^2, and the large system was essential for the existence of spirals. In Fig. 4 we demonstrate typical snapshots from the simulations, showing the variation of patterns as the hydrodynamic coupling strength is varied. These observations are quite similar to those features which have been revealed in spiral pattern formation in RB convection. As in the latter case, however, we are not able to identify a fundamental reason why the spirals disappear in the smaller systems.

In summary, we have considered effects of hydrodynamic interactions upon lamellar formation kinetics of thin block copolymer films. The stability analysis shows that the lamellar structure undergoes the skewed-varicose instability in the presence of the hydrodynamic interaction. We have also numerically demonstrated the existence of spiral and target patterns.

[1] See, for instance, I.W. Hamley, *The Physics of Block Copolymers* (Oxford University Press, Oxford, 1998).

[2] P. Manneville, *Dissipative Structures and Weak Turbulence* (Academic, New York, 1990).

[3] Y. Shiwa, T. Taneike, and Y. Yokojima, Phys. Rev. Lett. **77**, 4378 (1996); J.J. Christensen and A.J. Bray, Phys. Rev. E **58**, 5364 (1998).

[4] Y. Shiwa, Phys. Lett. A **228**, 279 (1997).

[5] Y. Oono and Y. Shiwa, Mod. Phys. Lett. B **1**, 49 (1987); M. Bahiana and Y. Oono, Phys. Rev. A **41**, 6763 (1990).

[6] L. Leibler, Macromolecules **13**, 1602 (1980); T. Ohta and K. Kawasaki, *ibid.* **19**, 2621 (1986).

[7] A. Zippelius and E.D. Siggia, Phys. Fluids **26**, 2905 (1983); P. Manneville, J. Phys. (Paris) **44**, 759 (1983).

[8] M.C. Cross and A.C. Newell, Physica D **10**, 299 (1984).

[9] H.S. Greenside and M.C. Cross, Phys. Rev. A **31**, 2492 (1985).

[10] G. Arfken, *Mathematical Method for Physicists* (Academic, New York, 1985).

[11] G. Sigaud, C.W. Garland, H.T. Nguyen, D. Roux, and S.T. Milner, J. Phys. II **3**, 1343 (1993); see also F. Nallet, D. Roux, and J. Prost, J. Phys. (France) **50**, 3147 (1989).

[12] P.I.C. Teixeira and B.M. Mulder, Phys. Rev. E **55**, 3789 (1997); Y. Oono, *ibid.* **55**, 3792 (1997).

[13] E. Bodenschatz, J.R. de Bruyn G. Ahlers, and D.S. Cannell, Phys. Rev. Lett. **67**, 3078 (1991); M. Assenheimer and V. Steinberg, *ibid.* **70**, 3888 (1993); S.W. Morris, E. Bodenschatz, D.S. Cannell, and G. Ahlers, *ibid.* **71**, 2026 (1993); and for recent development, see W. Pesch, Chaos **6**, 348 (1996).

[14] M.C. Cross and Y. Tu, Phys. Rev. Lett. **75**, 834 (1995), and references therein.

[15] E.D. Siggia and A. Zippelius, Phys. Rev. Lett. **47**, 835 (1981).

[16] Y. Oono and S. Puri, Phys. Rev. Lett. **58**, 836 (1987).